

# RSC Advances



This is an *Accepted Manuscript*, which has been through the Royal Society of Chemistry peer review process and has been accepted for publication.

*Accepted Manuscripts* are published online shortly after acceptance, before technical editing, formatting and proof reading. Using this free service, authors can make their results available to the community, in citable form, before we publish the edited article. This *Accepted Manuscript* will be replaced by the edited, formatted and paginated article as soon as this is available.

You can find more information about *Accepted Manuscripts* in the [Information for Authors](#).

Please note that technical editing may introduce minor changes to the text and/or graphics, which may alter content. The journal's standard [Terms & Conditions](#) and the [Ethical guidelines](#) still apply. In no event shall the Royal Society of Chemistry be held responsible for any errors or omissions in this *Accepted Manuscript* or any consequences arising from the use of any information it contains.

# Highly Stable Ni/SiC Catalyst Modified by Al<sub>2</sub>O<sub>3</sub> for CO Methanation Reaction

Guojing Jin<sup>a,b</sup>, Fangna Gu<sup>b,\*</sup>, Qing Liu<sup>b</sup>, Xiaoyan Wang<sup>b</sup>,

Lihua Jia<sup>a,\*</sup>, Guangwen Xu<sup>b</sup>, Ziyi Zhong<sup>c</sup>, and Fabin Su<sup>b,\*</sup>

<sup>a</sup> *College of Chemistry and Chemical Engineering, Qiqihaer University, Qiqihaer 161006, Heilongjiang Province, China*

<sup>b</sup> *State Key Laboratory of Multiphase Complex Systems, Institute of Process Engineering, Chinese Academy of Sciences, Beijing 100190, China*

<sup>c</sup> *Institute of Chemical Engineering and Sciences, A\*star, 1 Pesek Road, Jurong Island 627833, Singapore*

\*Corresponding author: [fngu@ipe.ac.cn](mailto:fngu@ipe.ac.cn) (F. Gu), [jlh29@163.com](mailto:jlh29@163.com) (L. Jia), [fbsu@ipe.ac.cn](mailto:fbsu@ipe.ac.cn) (F. Su),

Tel.: +86-10-82544850, Fax: +86-10-82544851.

## Abstract

It is still a great challenge to prevent sintering of supported Ni catalysts in highly exothermic reactions. To address this problem, in this work, highly thermal conductive and stable SiC is explored as Ni catalyst support for CO methanation to produce synthetic natural gas; simultaneously, Al<sub>2</sub>O<sub>3</sub> is utilized to modify the SiC surface to enhance the interaction between metal and support and restrain Ni active component from sintering or loss during the reaction. A series of Ni/Al<sub>2</sub>O<sub>3</sub>-SiC catalysts were successfully prepared by the co-deposition-precipitation method. The catalysts were investigated by N<sub>2</sub> adsorption, XRD, SEM/EDS, TEM, XPS, H<sub>2</sub>-TPR, H<sub>2</sub>-TPD and TG. The elemental mapping images indicated that the introduced Al<sub>2</sub>O<sub>3</sub> particles were uniformly deposited on the surface of SiC support, which evidently enhanced the interaction between Ni and support by forming Ni-Al<sub>2</sub>O<sub>3</sub> complexes as proved by H<sub>2</sub>-TPR results. The Ni/Al<sub>2</sub>O<sub>3</sub>-SiC catalyst with an optimal amount of Al<sub>2</sub>O<sub>3</sub> content showed a high catalytic activity and strong resistance to sintering, which can be attributed to two main factors: (1) the addition of Al<sub>2</sub>O<sub>3</sub> can enhance the interactions between Ni and the support, thus inhibiting the migration of Ni particles on the support surface and improving the dispersion of them; (2) the superior heat conductivity of SiC can decrease the generation of hot spots in the catalyst bed.

Keywords: co-deposition-precipitation, SiC, Al<sub>2</sub>O<sub>3</sub>-modified, *CO methanation*

## 1 Introduction

Methanation of carbon oxides with hydrogen to produce methane has been widely used in many industrial processes such as substitute natural gas (SNG) synthesis, removal of trace amounts of CO from H<sub>2</sub>-rich feed gas or purification of the reformat gas for NH<sub>3</sub> synthesis and fuel cell application, etc.<sup>1,2</sup> In recent years, production of SNG from coal via syngas methanation approach has attracted much interest in China due to the increasing demand for natural gas and the wish for clean utilization of coal resources.<sup>3</sup> Methanation for SNG production is a highly exothermic reaction due to the high concentrations of carbon oxides: for every 1% CO and 1% CO<sub>2</sub> conversion, the temperature rise of the gas composition in a typical methanator is 74 °C and 60 °C, respectively.<sup>4</sup> The potential dramatic temperature increase may cause severe sintering of the catalyst, thus the design of catalysts with high stability at high temperature is necessary.

Ni-based catalysts are preferred for syngas methanation due to their low cost, good availability, high activity, and the best selectivity to methane as compared to other metals.<sup>5</sup> Many materials such as TiO<sub>2</sub>, Al<sub>2</sub>O<sub>3</sub>, CeO<sub>2</sub>, SiO<sub>2</sub>, YSZ and MgAl<sub>2</sub>O<sub>4</sub> have been tested as the supports of Ni catalysts.<sup>6-9</sup> However, these catalysts often suffer from fast sintering and deactivation due to the rapid heat accumulation on them during the methanation process. In order to improve the stability of Ni catalysts, various promoters,<sup>3, 10, 11</sup> supports and<sup>12-14</sup> preparation methods<sup>15, 16</sup> have been selected and tested. However, hot spots are still easily generated in the catalyst bed for the conventional catalysts due to their poor thermal conductivity. To solve this problem, a common way used in industry is to connect several methanation reactors in series and add numbers of intermediate gas coolers, and recycle the product gas to dilute the feed gas to control the reaction temperature. Hence, the whole process becomes quite complicated and difficult to control. Alternatively, highly thermo-conductive and thermo-stable materials can be employed as the support of CO methanation catalysts to

alleviate the problem.

Silicon carbide (SiC) possesses superior thermal stability, high heat conductivity and chemical inertness,<sup>17</sup> and has been used as catalyst support in many different reactions, including methane reforming<sup>18</sup> and combustion,<sup>19</sup> Fischer-Tropsch synthesis,<sup>20, 21</sup> isomerization<sup>22</sup> and dehydrogenation,<sup>23</sup> etc. However, the commercial SiC powders have very low specific surface areas, unfavorable for the dispersion of active components. In addition, due to the chemical inertness of SiC, it has weak interaction with metal particles which leads to the poor stability of catalyst. Recently, it has reported that SiC with high specific surface area has been synthesized by different methods, such as sol-gel method,<sup>24</sup> polycarbosilane pyrolysis,<sup>25</sup> porous carbon template,<sup>26</sup> and nanocasting method<sup>27, 28</sup> using mesoporous silica (SBA-15 or MCM-48) as hard templates, etc. However, the above mentioned methods still have their shortcomings, including high complexity in synthesis, high cost, and the obtained SiC still has to be surface-modified as catalyst support due to its chemical inertness.

Wang et al. reported that Al<sub>2</sub>O<sub>3</sub>-modified biomorphic SiC pellets could prevent the growth and loss of Ni particles due to the enhanced interaction between Ni and support.<sup>29</sup> Koo et al. verified that Al<sub>2</sub>O<sub>3</sub> coating could enhance Co dispersion due to the formation of adjacently interacting Co-Al<sub>2</sub>O<sub>3</sub> species.<sup>20</sup> However, SiC used in these studies was usually synthesized by specific method or needed surface modification such as pre-coating Al<sub>2</sub>O<sub>3</sub> prior to the use as catalyst support.

In this work, we report a different approach for the synthesis of Ni catalysts supported on SiC modified by Al<sub>2</sub>O<sub>3</sub> for CO methanation, in which the Ni and Al<sub>2</sub>O<sub>3</sub> components are deposited on the commercial SiC by co-deposition-precipitation method. The Al<sub>2</sub>O<sub>3</sub> amount introduced and its effects on enhancing the dispersion and thermostability of Ni particles are investigated in detail.

## 2 Experimental

### 2.1 Catalyst preparation

All chemicals with analytical grade including aluminum nitrate nonahydrate ( $\text{Al}(\text{NO}_3)_3 \cdot 9\text{H}_2\text{O}$ ), nickel(II) nitrate hexahydrate ( $\text{Ni}(\text{NO}_3)_2 \cdot 6\text{H}_2\text{O}$ ) and potassium hydroxide (KOH) were purchased from Sinopharm Chemical Reagent Co. Ltd., China, and used without further treatment. The commercial SiC (purity >98%, Pingxiang Ruize Silicon Ceramic Co. Ltd., China) was calcined at 500 °C in air for 2 h before use. The impurities in the commercial SiC were quite low in concentration analyzed by X-ray fluorescence (XRF) (see Table S1), and may have no impact to the catalytic reaction. Therefore, in this work, the SiC powder was used without further treatment. The Ni/Al<sub>2</sub>O<sub>3</sub>-SiC catalysts were prepared by the co-deposition-precipitation method. Typically, 3.50 g of the SiC support was added to a round bottom flask with 50 mL deionized water to form a slurry, then the obtained slurry was slowly heated to 60 °C in a water bath under vigorously stirring. Subsequently, 3.89 g of Ni(NO<sub>3</sub>)<sub>2</sub> · 6H<sub>2</sub>O and 1.83 g of Al(NO<sub>3</sub>)<sub>3</sub> · 9H<sub>2</sub>O were dissolved in 50 mL deionized water, respectively, followed by adding the above solutions into the slurry by dropwise in a parallel flow form, meanwhile 0.1 M KOH solution was concurrently added to control the pH value which was maintained at around 9.0. The slurry was stirred vigorously for 8 h and then cooled down to room temperature, and filtered under vacuum and washed several times with deionized water. The obtained product was then dried at 100 °C for 12 h and further calcined at 400 °C for 2 h in air with the heating rate of 2 °C min<sup>-1</sup>. The synthesized catalyst was denoted as 20Ni10Al70SiC with a NiO loading of 20 wt%, Al<sub>2</sub>O<sub>3</sub> of 10 wt% and SiC of 70 wt%. Likewise, other 20Ni<sub>x</sub>Al<sub>y</sub>SiC catalysts were also prepared with the Al<sub>2</sub>O<sub>3</sub> amount of 0, 5 and 20 wt% using the same method and denoted as 20Ni80SiC, 20Ni5Al75SiC and 20Ni20Al60SiC, respectively.

## 2.2. Catalyst characterization

N<sub>2</sub> adsorption/desorption isotherms were measured at -196 °C using a Quantachrome surface area & pore size analyzer NOVA 3200e. Prior to the measurement, the sample was degassed at 300 °C for 3 h under vacuum. The specific surface area was determined according to the Brunauer-Emmett-Teller (BET) method in the relative pressure range of 0.05–0.2. The pore size distribution (PSD) was calculated based on the Barrett-Joyner-Halenda (BJH) method using the adsorption isotherm branch. Thermogravimetric (TG) analysis was conducted to determine the deposited carbon content on a Seiko Instruments EXSTAR TG/DTA 6300. 10 mg of the sample was used and heated under air (200 mL min<sup>-1</sup>) from room temperature up to 1000 °C (10 °C min<sup>-1</sup>). X-ray diffraction (XRD) patterns were recorded on a PANalytical X'Pert PRO MPD with a step of 0.03° using Cu K $\alpha$  radiation ( $\lambda=1.5418$  Å) at 40 kV and 40 mA. The crystal size of the sample was estimated using the Debye-Scherrer equation. The microscopic feature of the samples was observed by field emission scanning electron microscope (SEM) (SU-8000, HITACHI, Japan) and transmission electron microscopy (TEM) (JEM-2010F, JEOL, Japan). Before TEM measurement, the H<sub>2</sub>-reduced catalysts were cooled to room temperature in H<sub>2</sub> flow and then passivated in 1 vol% O<sub>2</sub>/Ar gas mixture for 30 min to prevent bulk oxidation of the Ni nanoparticles. Energy dispersed spectroscopy (EDS) (INCA X-MAX, JEOL, Oxford, England) was conducted to determine the elemental composition and distribution. The surface chemical composition was analyzed by an X-ray photoelectron spectroscopy (XPS) conducted on a VG ESCALAB 250 spectrometer (Thermo Electron, U.K.) with a non-monochromatized Al K $\alpha$  X-Ray source (1486 eV). H<sub>2</sub> temperature-programmed reduction (H<sub>2</sub>-TPR) and H<sub>2</sub> temperature-programmed desorption (H<sub>2</sub>-TPD) were carried out on Quantachrome Automated chemisorption analyzer (ChemBET pulsar TPR/TPD). For H<sub>2</sub>-TPR, 0.1 g sample was loaded in a quartz U-tube and heated from room

temperature to 300 °C at 10 °C min<sup>-1</sup> and maintained for 1 h under He flow. Then, the sample was cooled to room temperature, followed by heating to 1000 °C with a heating rate of 10 °C min<sup>-1</sup> in 10 vol% H<sub>2</sub>/Ar flow (30 mL min<sup>-1</sup>). For H<sub>2</sub>-TPD, 0.2 g catalyst was used and reduced in situ in a H<sub>2</sub>/Ar flow at 600 °C for 2 h previously. Then the sample was cooled to room temperature and saturated with H<sub>2</sub>. After removing the physically adsorbed H<sub>2</sub> by flushing with Ar for 2 h, the sample was heated to 1000 °C using a ramping rate of 10 °C min<sup>-1</sup> in an Ar flow (30 mL min<sup>-1</sup>). The consumed or desorbed H<sub>2</sub> was detected continuously as a function of increasing temperature using a thermal conductivity detector (TCD). The number of surface Ni sites per unit mass of catalyst was determined by means of H<sub>2</sub>-TPD assuming the adsorption stoichiometry of H/Ni=1:1. The peak area of H<sub>2</sub>-TPD profile was normalized to that of H<sub>2</sub>-TPR of a standard CuO sample. The dispersion of Ni was calculated based on the volume of chemisorbed H<sub>2</sub> using the following simplified equation:<sup>30</sup>

$$D(\%) = \frac{2 \times V_{ad} \times M \times SF}{m \times P \times V_m \times d_r} \times 100$$

Where  $V_{ad}$  (mL) represents the volume of chemisorbed H<sub>2</sub> under standard temperature and pressure (STP) conditions measured in the TPD procedure;  $m$  is the sample weight (g);  $M$  is the molecular weight of Ni (58.69 g mol<sup>-1</sup>);  $P$  is the weight fraction of Ni in the sample determined by ICP;  $SF$  is the stoichiometric factor (the Ni:H molar ratio in the chemisorption) which is taken as 1 and  $V_m$  is molar volume of H<sub>2</sub> (22414 mL mol<sup>-1</sup>) at STP;  $d_r$  is the reduction degree of Ni calculated based on H<sub>2</sub>-TPR results.

### 2.3. Catalytic activity measurements

The catalytic measurements are similar to our previous work.<sup>31-35</sup> Typically, the CO methanation reactions were carried out in a fixed bed reactor at 0.1 MPa, with the temperature range of 260 to

550 °C. The influence of mass transfer was examined and eliminated before the catalytic tests. 0.2 g of catalyst sample (20–40 mesh) diluted with 4.0 g quartz sands (20–40 mesh) was uploaded in a quartz tube with a diameter of 8 mm in the reactor. The addition of quartz sands was to avoid the generation of hot spots in the catalyst bed. A thermocouple was placed outside of the reactor tube near the middle position of the catalyst bed to measure and monitor the reaction temperature. Prior to the reaction, the catalysts were reduced at 600 °C in pure H<sub>2</sub> (100 mL min<sup>-1</sup>) for 2 h and then cooled to the starting reaction temperature in the same atmosphere, and then subjected to the mixed H<sub>2</sub> and CO as well as N<sub>2</sub> (as an internal standard) at a molar ratio of H<sub>2</sub>/CO/N<sub>2</sub>=3/1/1. The outlet gas stream from the reactor was cooled using a cold trap. The inlet and outlet gases were analyzed on line using a Micro GC 3000A (Agilent Technologies). The concentrations of H<sub>2</sub>, N<sub>2</sub>, CH<sub>4</sub> and CO in gas products were detected by a TCD detector connected with a Molecular Sieve column while the concentrations of CO<sub>2</sub>, C<sub>2</sub>H<sub>4</sub>, C<sub>2</sub>H<sub>6</sub>, C<sub>3</sub>H<sub>6</sub> and C<sub>3</sub>H<sub>8</sub> were analyzed using another TCD connected with a Plot Q column. A life time test of CO methanation was performed at 550 °C and 0.1 MPa. Hydrothermal treatment for catalysts aging was also carried out in this fixed bed quartz tube reactor at 700 °C and 0.1 MPa for 10 h, the catalysts after 90 vol% H<sub>2</sub>O/H<sub>2</sub> treated were labeled as 20Ni80SiC-HT and 20Ni10Al70SiC-HT, respectively. The CO conversion, CH<sub>4</sub> selectivity and yield are defined as follows:

$$\text{CO conversion: } X_{\text{CO}}(\%) = \frac{F_{\text{CO},in} - F_{\text{CO},out}}{F_{\text{CO},in}} \times 100$$

$$\text{CH}_4 \text{ selectivity: } S_{\text{CH}_4}(\%) = \frac{F_{\text{CH}_4,out}}{F_{\text{CO},in} - F_{\text{CO},out}} \times 100$$

$$\text{CH}_4 \text{ yield: } X_{\text{CO}}(\%) = \frac{F_{\text{CO},in} - F_{\text{CO},out}}{F_{\text{CO},in}} \times 100$$

Here,  $X$  is the conversion of CO,  $S$  is the selectivity of CH<sub>4</sub>,  $Y$  is the yield of CH<sub>4</sub>,  $F_{i, in}$  and  $F_{i, out}$  are the volume flow rates of species  $i$  ( $i = \text{CO}$  or  $\text{CH}_4$ ) at the inlet and outlet.

The rate and activation energy for CO methanation over the catalyst were determined using the

reactor above at 0.1 MPa. 0.5 g catalyst sample (20–40 mesh) diluted with 3.0 g quartz sands (20–40 mesh) was used. The experiments were performed with different total gas flow of 50, 100 and 200 mL min<sup>-1</sup> in the temperature range of 190–220 °C. The rate was determined using the following equation:<sup>6</sup>

$$\text{Rate}(r) = \frac{F_{CO} \times X_{CO}}{W} = \frac{X_{CO}}{W/F_{CO}}$$

Where  $F_{CO}$  represents the flow of the CO in mol s<sup>-1</sup>,  $W$  is the weight of the catalyst in g, and  $X_{CO}$  the CO conversion. The variations of  $X_{CO}$  with  $W/F_{CO}$  were plotted, and then the rates of reaction were calculated at various temperatures from the slope of linear portion. The activation energy was calculated using the Arrhenius equation.

### 3. Results and Discussion

#### 3.1. Characterization of the catalysts

##### 3.1.1. Nitrogen adsorption analysis

The surface area, pore volume and pore size of the as-calcined 20Ni<sub>x</sub>Al<sub>y</sub>SiC catalysts are summarized in Table 1. As the specific surface area and pore volume of SiC are as low as 1 m<sup>2</sup> g<sup>-1</sup> and 0.003 cm<sup>3</sup> g<sup>-1</sup>, respectively (See Table S1), the surface area of all the catalysts is increased obviously which should be due to the increased surface roughness after NiO particles loading. Comparing with 20Ni80SiC, the as-calcined 20Ni<sub>x</sub>Al<sub>y</sub>SiC ( $x \geq 5$ ) catalysts with Al<sub>2</sub>O<sub>3</sub> modification show higher specific surface areas, which should be attributed to the deposition of mesoporous Al<sub>2</sub>O<sub>3</sub> on SiC surface, as proved by the pore size distribution curves (Fig. S1). Among all the 20Ni<sub>x</sub>Al<sub>y</sub>SiC catalysts, 20Ni20Al60SiC has the largest specific surface area, indicating thick Al<sub>2</sub>O<sub>3</sub> depositional layer formed on SiC surface which may not be beneficial to thermal transmission on this catalyst.

### 3.1.2. XRD analysis.

Fig. 1A displays the XRD patterns of all the freshly reduced catalysts. It can be seen that the support shows a group of distinct peaks assigned to  $\beta$ -SiC phase (JCPDS 74-1302). The diffraction peaks at  $44.5^\circ$ ,  $51.9^\circ$ , and  $76.4^\circ$  in the pattern of 20Ni80SiC are indexed to (111), (200), (220) planes of face centered cubic Ni (JCPDS 70-1849), respectively, and these peaks become broader in those of 20Ni<sub>x</sub>Al<sub>y</sub>SiC catalysts as shown in Fig 1B. The mean sizes of Ni crystallites are estimated from the (111) diffraction according to Scherrer equation. As shown in Table 1, compared with 20Ni80SiC, the calculated Ni particle sizes of 20Ni<sub>x</sub>Al<sub>y</sub>SiC catalysts become obviously smaller. Among them, 20Ni10Al70SiC has the smallest Ni size, indicating that the introduction of proper amount of Al<sub>2</sub>O<sub>3</sub> can improve the dispersion of NiO particles. In addition, no characteristic peaks of Al<sub>2</sub>O<sub>3</sub> phases can be identified for all the 20Ni<sub>x</sub>Al<sub>y</sub>SiC samples, which should be due to its low content and well dispersion, or it may be amorphous.<sup>20</sup>

### 3.1.3. SEM and TEM observations

SEM images of the SiC support and the freshly reduced 20Ni80SiC and 20Ni10Al70SiC are displayed in Fig. 2. It can be seen in Fig. 2a that the SiC support comprises micron-sized particles with a very smooth surface and relatively regular shape. In contrast, in 20Ni80SiC, there are many relatively small and irregular particles that are randomly dispersed on SiC surface, and some of them aggregate together (Fig. 2b). As there is no other component in 20Ni80SiC, we can easily infer these particles are Ni particles. For 20Ni10Al70SiC, after modification of the SiC surface with Al<sub>2</sub>O<sub>3</sub>, it is seen that the large SiC particles are covered by a layer of small particles (Fig. 2c), indicating the well dispersed Al<sub>2</sub>O<sub>3</sub> and Ni particles on the SiC surface. This well dispersed layer is supposed to be built up through the chemical reactions between the negatively charged surface sites of SiC particles and the positively charged aluminium hydroxide or oxide during which the support

can attain  $\text{Al}_2\text{O}_3$ -like surface.<sup>36</sup> The element mappings of 20Ni10Al70SiC are also shown in Fig. 3, which confirm that Ni and  $\text{Al}_2\text{O}_3$  components are homogeneously dispersed on SiC support. In addition, the surface molar ratio of Ni and Al calculated from the EDS characterization results ( $\text{Ni}/\text{Al} = 2.7$ ) is consistent with the nominal value, indicating they are well dispersed on the surface of SiC.

To compare the size distribution of Ni particles in the different catalysts, Fig. 4 shows TEM images of the support and the freshly reduced catalysts. By comparing the images of the support and the catalysts, Ni particles can be clearly distinguished due to the different contrast. It can be seen that, 20Ni10Al70SiC has smaller Ni particles with narrower size distribution than 20Ni80SiC, and their average Ni particle sizes are calculated to be 15.2 nm and 8.4 nm, respectively, proving that the introduction of  $\text{Al}_2\text{O}_3$  can improve the dispersion of NiO particles on SiC support. These results are consistent with the calculated values from XRD patterns in the range of allowable error by considering the difference between these two methods of measurement. The HRTEM image of 20Ni10Al70SiC is also shown in Fig. 4d. The observed lattice spacing of ca. 0.20 nm is attributed to the Ni (1 1 1) plane, which is closely related to the active sites for the methanation reaction.<sup>30</sup> The lattice spacing of ca. 0.25 nm is corresponding to the (0 0 6) plane of SiC, and the other parts marked in the image where there is no lattice spacing observed should be covered with  $\text{Al}_2\text{O}_3$  component. Obviously, we can see that Ni particles are mainly dispersed on the  $\text{Al}_2\text{O}_3$ -modified SiC surface.

#### 3.1.4. XPS analysis

The Ni  $2p_{3/2}$  XPS spectra of the freshly reduced 20Ni80SiC and 20Ni10Al70SiC are shown in Fig. 5a. It can be seen that the binding energy of  $\text{Ni}^0$  in 20Ni10Al70SiC (852.9 eV) is shifted to a higher binding energy as compared with that in 20Ni80SiC (852.5 eV), probably related to the enhanced

interaction between Ni and Al<sub>2</sub>O<sub>3</sub>.<sup>37</sup> Comparing with 20Ni80SiC, 20Ni10Al70SiC shows a weaker Ni<sup>0</sup> peak but a stronger Ni<sup>2+</sup> peak, indicating that the Ni particles of 20Ni10Al70SiC are more easily oxidized due to their high dispersion.<sup>38</sup> The observation of Ni oxide state (Ni<sup>2+</sup>) should be ascribed to the oxidation of surface Ni after exposure to air during the sample transfer. Fig. 5b shows the O 1s spectra of these two reduced Ni catalysts which can be fitted into two sub-peaks: the one with low binding energy peak is assigned to the surface lattice oxygen (O<sub>I</sub>), and the one with high binding energy to the adsorbed oxygen (O<sub>II</sub>).<sup>39</sup> The adsorbed oxygen species is derived from oxygen vacancies which is closely related to oxygen mobility in the catalyst.<sup>40</sup> We can see that both the binding energy of O<sub>I</sub> and O<sub>II</sub> of 20Ni10Al70SiC are shifted to higher values as compared with that of 20Ni80SiC (O<sub>I</sub>: 530.80 eV → 531.03 eV, O<sub>II</sub>: 532.08 eV → 532.17 eV), indicating the stronger interaction between Ni and Al<sub>2</sub>O<sub>3</sub>. In addition, the increased percentage of O<sub>I</sub> species from 0.43 of 20Ni80SiC to 0.58 of 20Ni10Al70SiC calculated by integration of the peak areas should be ascribed to the impact of oxygen in Al<sub>2</sub>O<sub>3</sub>.

### 3.1.5. H<sub>2</sub>-TPR analysis

Fig. 6a displays TPR profiles of all the samples. It is obviously that the SiC support shows no obvious reduction peak within the test temperature range. 20Ni80SiC displays only one peak centered at 436 °C, which is associated to the reduction of NiO species weakly interacted with the SiC support.<sup>7</sup> For 20Ni5Al75SiC, the reduction peak moves to higher temperature (500 °C) and becomes broader, which should be assigned to the reduction of β-type NiO species with Al-rich mixed oxide phase,<sup>7, 15</sup> indicating the enhanced interaction between NiO and the composite support after introduction of Al<sub>2</sub>O<sub>3</sub>. This is because the introduced Al<sub>2</sub>O<sub>3</sub> can be well coated on SiC to form a composite support, which is useful to increase surface area capable of bearing with high dispersion of NiO on it. With the increase of Al<sub>2</sub>O<sub>3</sub> content on the SiC support, the reduction peaks

of 20Ni10Al70SiC tend to be overlapped with a shoulder peak appeared at 744 °C, which can be assigned to the reduction of  $\gamma$ -type NiO species<sup>7, 15</sup> with the nickel aluminum spinel structure. In addition, there is a new weak reduction peak appeared at about 300 °C, which is assigned to the reduction of NiO species in the form of highly dispersed NiO clusters on the surface of Al<sub>2</sub>O<sub>3</sub> and/or SiC. For 20Ni20Al60SiC, the reduction peaks at high temperature region are partially overlapped, suggesting that more NiO species which are difficult to be reduced are generated with the further increase of Al<sub>2</sub>O<sub>3</sub> content.<sup>20</sup> It is obviously that the main reduction peaks of all the 20Ni<sub>x</sub>Al<sub>y</sub>SiC ( $x \geq 5$ ) catalysts are shifted to higher temperature due to the strong interaction between Ni and Al<sub>2</sub>O<sub>3</sub>. However, excessive Al<sub>2</sub>O<sub>3</sub> is found to be harmful to the reducibility of the prepared Ni-based catalyst.

### 3.1.6. H<sub>2</sub>-TPD analysis

Fig. 6b shows the H<sub>2</sub>-TPD profiles of the four reduced catalysts. For 20Ni80SiC, the H<sub>2</sub>-TPD profile shows only one desorption peak centered at around 200 °C, attributing to the desorption of chemisorbed H<sub>2</sub> on the Ni particles with high density surface defects, which usually serves as the capture centers for hydrogen with low activation energy of hydrogen dissociation.<sup>41</sup> For 20Ni5Al75SiC and 20Ni10Al70SiC, the intensity of this peak is increased obviously as compared with that of 20Ni80SiC, indicating that the addition of proper amount of Al<sub>2</sub>O<sub>3</sub> can increase the dispersion of Ni nanoparticles. For 20Ni20Al60SiC, a new shoulder peak appeared at around 300 °C becomes obvious, which can be assigned to the desorption of hydrogen adsorbed on the nickel species deposited on the thick Al<sub>2</sub>O<sub>3</sub> layer.

The hydrogen uptakes of the four reduced catalysts and Ni dispersion calculated based on the H<sub>2</sub>-TPR and H<sub>2</sub>-TPD results are listed in Table 1. The results reveal that 20Ni10Al70SiC has the highest total H<sub>2</sub> uptake of 141.4  $\mu\text{mol g}^{-1}$  and Ni dispersion of 10.56 %, indicating the introduction

of proper amount of  $\text{Al}_2\text{O}_3$  can improve the dispersion of Ni particles, and thus enhance  $\text{H}_2$  uptake of the catalyst, which is important to improve the activity of the catalyst for CO methanation.

### 3.2. Catalytic performances of the catalysts

#### 3.2.1. CO Methanation.

CO methanation was first carried out in the temperature range of 260–550 °C at a WHSV of 30000  $\text{mL g}^{-1} \text{h}^{-1}$  and 0.1 MPa, and the results are shown in Fig. 7a–c. For 20Ni80SiC, the catalytic activity is very poor below 300 °C, and the CO conversion over it reaches the thermodynamics equilibrium value when the temperature is as high as 450 °C. Comparing with 20Ni80SiC, the addition of  $\text{Al}_2\text{O}_3$  can considerably improve the catalyst's low temperature activities. The CO conversion over all the 20Ni $x$ Al $y$ SiC ( $x \geq 5$ ) catalysts can reach the thermodynamics equilibrium value in the temperature range of 320–350 °C. The activities of all the catalysts beyond 450 °C become low again because the CO methanation is a highly exothermic reaction with thermodynamic limit.<sup>42</sup> The addition of  $\text{Al}_2\text{O}_3$  also can increase  $\text{CH}_4$  selectivity of the catalyst as shown in Fig. 7b. The maximal  $\text{CH}_4$  yields over both 20Ni10Al70SiC and 20Ni20Al70SiC can reach 89% at a relative low temperature of 340 °C, while that over 20Ni80SiC is just 78% even at 430 °C (Fig. 7c). Clearly, the addition of proper amount of  $\text{Al}_2\text{O}_3$  (10%) can remarkably enhance the low temperature activity of the catalyst at atmospheric pressure; however, further increasing the amount of  $\text{Al}_2\text{O}_3$  up to 20% results in little change in the activity of the catalyst. Happel et al. found that the slowest step in the methanation reaction was the hydrogenation of  $\text{CH}_x$  species, and the concentration of adsorbed hydrogen atoms on the surface was the determining factor of this hydrogenation reaction.<sup>43</sup> Combining with the aforementioned  $\text{H}_2$ -TPD results, we can conclude that the much improved activity of 20Ni10Al70SiC for CO methanation can be attributed to the

enhanced H<sub>2</sub> uptakes caused by the high dispersion of Ni particles, in which case more active sites are generated. The catalytic performance evaluation results indicate that the addition of Al<sub>2</sub>O<sub>3</sub> by co-deposition-precipitation method is effective in improving the catalytic activities through the formation of a uniformly dispersed Al<sub>2</sub>O<sub>3</sub> on SiC which can facilitate the high dispersion of Ni particles.

### 3.2.2. Apparent activation energies of the catalysts in CO methanation

The apparent activation energies of CO methanation over all the catalysts were determined and the Arrhenius plots are shown in Fig. 8. The results show that the activation energies decrease in the order of 20Ni80SiC > 20Ni5Al75SiC > 20Ni20Al60SiC > 20Ni10Al70SiC, which is in good agreement with their activity trend in CO methanation at atmospheric pressure. This is because for Ni-based catalysts, the rate-controlling step in the methanation reaction is the hydrogenation of CH<sub>x</sub> species.<sup>43</sup> To promote catalytic activity, it is crucial to realize a fast removal of these surface CH<sub>x</sub> species by surface dissociated hydrogen. The smaller Ni particles with more surface defects can serve as capture traps for surface hydrogen and reduce the activation energy of hydrogen dissociation.<sup>41</sup> Therefore, the smallest activation energy obtained on 20Ni10Al70SiC should be due to the smallest Ni particle size which can facilitate the adsorption and dissociation of hydrogen. In addition, to obtain accurate TOF<sub>CO</sub> values, WHSH was literately increased to 120000 mL g<sup>-1</sup> h<sup>-1</sup> to lower CO conversion at 260 °C (see Fig. S3). The calculated TOF<sub>CO</sub> values based on the CO conversion at this temperature and the H<sub>2</sub> adsorption amount are listed in Table 1. It can be seen that 20Ni10Al70SiC possesses the highest TOF<sub>CO</sub> value (0.158 S<sup>-1</sup>), which further demonstrates that the optimal amount of Al<sub>2</sub>O<sub>3</sub> introduced here is about 10%.

### 3.3. Stability of the catalysts

The lifetime test is important for evaluation of a catalyst; particularly, maintaining the activity and stability of the catalyst under harsh reaction conditions is crucial for the industrial process. Therefore, we carried out the 120 h lifetime tests for 20Ni80SiC, 20Ni5Al75SiC and 20Ni10Al70SiC at 550 °C, 0.1MPa and different WHSVs, and the results are shown in Fig. 9. For 20Ni80SiC, the activity remains stable within the first 20 h test at 550 °C with WHSV of 30,000 mL g<sup>-1</sup> h<sup>-1</sup> and even in the second 20 h test with increased WHSV of 60,000 mL g<sup>-1</sup> h<sup>-1</sup>, indicating a relatively good thermal stability of it due to the good thermal conductivity of SiC support. However, it tends to decrease slightly in the third 20 h test (total time 60 h) at 90,000 mL g<sup>-1</sup> h<sup>-1</sup>. Especially, the significant decline can be seen at extreme high WHSV of 120,000 mL g<sup>-1</sup> h<sup>-1</sup> after 60 h (total time 120 h). In contrast, the catalytic performance of 20Ni5Al75SiC and 20Ni10Al70SiC remain stable at every step during the whole 120 h lifetime test, indicating that Ni particles can be strongly anchored on the support by introducing a small amount of Al<sub>2</sub>O<sub>3</sub>. In addition, the Ni/Al<sub>2</sub>O<sub>3</sub>-SiC catalyst with optimal amount of Al<sub>2</sub>O<sub>3</sub> show higher activity and stability than those Ni-based catalysts without adding promoter supported on the conventional material such as bentonite,  $\alpha$ -Al<sub>2</sub>O<sub>3</sub>.<sup>34, 35</sup>

#### 3.4. Characterization of the used catalysts

The TEM images of the used 20Ni80SiC, 20Ni5Al75SiC and 20Ni10Al70SiC catalysts are shown in Fig. 10a–c. The agglomeration of Ni particles in the used 20Ni80SiC is very serious compared with the freshly reduced 20Ni80SiC (see Fig. 4b), which should be due to the easy migration of Ni particles caused by the poor interaction with the support. In contrast, Ni particles are still well dispersed in the used 20Ni5Al75SiC and 20Ni10Al70SiC. Ni particle sizes of these used catalysts were also measured by XRD, and the calculated values are 18.5, 9.3 and 7.5 nm,

respectively (see Fig. S4). Although Ni particle sizes of the used catalysts are bigger than those of the fresh catalysts (see Table 1), the used 20Ni5Al75SiC and 20Ni10Al70SiC catalyst still possess much smaller Ni particle sizes than the freshly reduced 20Ni80SiC. In addition, some filamentous carbon can be clearly seen on the surface of the used 20Ni80SiC (Fig. S5). The amount of carbon deposited on both of the used 20Ni80SiC and 20Ni10Al70SiC is further measured by TG analysis, and the results are presented in Fig. 10d. The carbon content over them is estimated to be 2.0 and 1.4 wt% respectively, suggesting the latter has a stronger coke resistance than the former. In addition, no new diffraction peak corresponding to graphitic carbon is observed in the XRD patterns of the used catalysts (see Fig. S4), probably because the amount of this filamentous carbon is below the detection limit of XRD or they mainly exist in the form of amorphous.

### *3.5. Catalytic properties of the catalysts for CO methanation after hydrothermal treatment*

Considering water is one of the byproducts in CO methanation and additional steam is often mixed into the feed gas atmosphere to avoid the generation of hot spots in the catalyst bed and to reduce carbon deposition in industry,<sup>44</sup> the hydrothermal stability of both 20Ni80SiC and 20Ni10Al70SiC was examined. These two catalysts after hydrothermal treatment are labeled by adding a “HT” suffix, and the activity evaluation results are shown in Fig. 11. Compared with the fresh catalysts, the catalytic activities of 20Ni80SiC-HT and 20Ni10Al70SiC-HT are declined in different extent. The drastic decrease of catalytic activity obtained on 20Ni80SiC-HT should be due to the poor interaction of Ni particles with the SiC support. On the contrary, 20Ni10Al70SiC-HT still shows relatively high activity for CO methanation, indicating the introduction of proper amount of Al<sub>2</sub>O<sub>3</sub> is useful to stabilize Ni particles on SiC. The mean particle size of Ni in the two catalysts was also estimated using XRD analysis (see Fig. S4). It can be found that Ni particle size grows

from 13.3 nm to 37.5 nm in 20Ni80SiC-HT, while the change in 20Ni10Al70SiC-HT is from 5.5 nm to 15.3 nm. The Ni particle size of 20Ni10Al70SiC-HT is still smaller than that of 20Ni80SiC, further suggesting the better stability of 20Ni10Al70SiC than 20Ni80SiC. In addition, it can be found that 20Ni10Al70SiC also show a better hydrothermal stability than the Ni/ $\gamma$ -Al<sub>2</sub>O<sub>3</sub> catalyst by comparing with our previous research results,<sup>7</sup> which should be ascribed to the superior thermal stability of SiC support.

#### 4. Conclusions

In this work, a series of Ni/Al<sub>2</sub>O<sub>3</sub>-SiC catalysts are successfully prepared by the co-deposition-precipitation method. The XRD and EDS characterization results indicate that the introduced Al<sub>2</sub>O<sub>3</sub> is evenly deposited on the surface of SiC and has a strong binding with Ni particles, leading to the improved dispersion and less aggregation of Ni particles. Thus the prepared Ni/SiC-Al<sub>2</sub>O<sub>3</sub> exhibits both high catalytic performance and high stability in CO methanation reaction. It is found that the catalyst resistance to carbon deposition becomes stronger only with the optimal amount of Al<sub>2</sub>O<sub>3</sub> content. With the introduction of excessive Al<sub>2</sub>O<sub>3</sub>, it will generate Ni-Al<sub>2</sub>O<sub>3</sub> complex that is more difficult to be reduced, and not conducive to the catalytic performance as proven in the case of the 20Ni20Al60SiC catalyst. Our work demonstrates that the Al<sub>2</sub>O<sub>3</sub>-modified low specific surface SiC is a promising support candidate for CO methanation to produce SNG.

#### Acknowledgments

The authors gratefully acknowledge the supports from the National Natural Science Foundation of China (nos. 21476238 and 21206173), the National Basic Research Program (no. 2014CB744306), the Fund of State Key Laboratory of Multiphase Complex Systems (nos.MPCS-2014-D-03 and MPCS-2015-A-06), the National High Technology Research and

Development Program 863 (no. SS2015AA050502), “Strategic Priority Research Program” of the Chinese Academy of Sciences (nos. XDA07010100 and XDA07010200), and the National Research Foundation of Singapore (M4098015.121).

## References

1. M. B. I. Choudhury, S. Ahmed, M. A. Shalabi and T. Inui, *Appl. Catal., A*, 2006, **314**, 47-53.
2. A. M. Abdel-Mageed, S. Eckle, H. G. Anfang and R. J. Behm, *J. Catal.*, 2013, **298**, 148-160.
3. Q. Liu, F. Gu, X. Lu, Y. Liu, H. Li, Z. Zhong, G. Xu and F. Su, *Appl. Catal., A*, 2014, **488**, 37-47.
4. G. Zhang, T. Sun, J. Peng, S. Wang and S. Wang, *Appl. Catal., A*, 2013, **462-463**, 75-81.
5. G. A. Mills and F. W. Steffgen, *Catal. Rev.*, 1974, **8**, 159-210.
6. V. M. Shinde and G. Madras, *AIChE J.*, 2014, **60**, 1027-1035.
7. J. Gao, C. Jia, J. Li, M. Zhang, F. Gu, G. Xu, Z. Zhong and F. Su, *J. Nat. Gas Chem.*, 2013, **22**, 919-927.
8. P. Panagiotopoulou, D. I. Kondarides and X. E. Verykios, *Appl. Catal., B*, 2009, **88**, 470-478.
9. A. L. Kustov, A. M. Frey, K. E. Larsen, T. Johannessen, J. K. Nørskov and C. H. Christensen, *Appl. Catal., A*, 2007, **320**, 98-104.
10. R.-f. Wu, Y. Zhang, Y.-z. Wang, C.-g. Gao and Y.-x. Zhao, *J. Fuel Chem. Technol.*, 2009, **37**, 578-582.
11. D. Hu, J. Gao, Y. Ping, L. Jia, P. Gunawan, Z. Zhong, G. Xu, F. Gu and F. Su, *Ind. Eng. Chem. Res.*, 2012, **51**, 4875-4886.
12. J. Zhang, Z. Xin, X. Meng and M. Tao, *Fuel*, 2013, **109**, 693-701.
13. B. Lu and K. Kawamoto, *Fuel*, 2013, **103**, 699-704.
14. H. Lu, X. Yang, G. Gao, K. Wang, Q. Shi, J. Wang, C. Han, J. Liu, M. Tong, X. Liang and C. Li, *Int. J. Hydrogen Energy*, 2014, **39**, 18894-18907.
15. A. Zhao, W. Ying, H. Zhang, H. Ma and D. Fang, *Catal. Commun.*, 2012, **17**, 34-38.
16. J. Zhang, Y. Bai, Q. Zhang, X. Wang, T. Zhang, Y. Tan and Y. Han, *Fuel*, 2014, **132**, 211-218.
17. M. Ledoux and C. Pham-Huu, *CATTECH*, 2001, **5**, 226-246.
18. J. M. García-Vargas, J. L. Valverde, A. de Lucas-Consuegra, B. Gómez-Monedero, F. Dorado and P. Sánchez, *Int. J. Hydrogen Energy*, 2013, **38**, 4524-4532.
19. X. Guo, G. Zhi, X. Yan, G. Jin, X. Guo and P. Brault, *Catal. Commun.*, 2011, **12**, 870-874.
20. H.-M. Koo, B. S. Lee, M.-J. Park, D. J. Moon, H.-S. Roh and J. W. Bae, *Catal. Sci. Technol.*, 2014, **4**, 343-351.
21. A. R. de la Osa, A. De Lucas, J. Díaz-Maroto, A. Romero, J. L. Valverde and P. Sánchez, *Catal. Today*, 2012, **187**, 173-182.
22. C. Pham-Huu, P. D. Gallo, E. Peschiera and M. J. Ledoux, *Appl. Catal., A*, 1995, **132**, 77-96.
23. M. E. Harlin, A. O. I. Krause, B. Heinrich, C. Pham-Huu and M. J. Ledoux, *Appl. Catal., A*, 1999, **185**, 311-322.
24. G.-Q. Jin and X.-Y. Guo, *Microporous Mesoporous Mater.*, 2003, **60**, 207-212.
25. V. G. Pol, S. V. Pol and A. Gedanken, *Chem. Mater.*, 2005, **17**, 1797-1802.
26. Z. Liu, W. Shen, W. Bu, H. Chen, Z. Hua, L. Zhang, L. Li, J. Shi and S. Tan, *Microporous Mesoporous Mater.*, 2005, **82**, 137-145.
27. N. Leventis, A. Sadekar, N. Chandrasekaran and C. Sotiriou-Leventis, *Chem. Mater.*, 2010, **22**, 2790-2803.
28. A.-H. Lu, W. Schmidt, W. Kiefer and F. SCHÜTH, *J. Mater. Sci.*, 2005, **40**, 5091-5093.
29. Q. Wang, W.-Z. Sun, G.-Q. Jin, Y.-Y. Wang and X.-Y. Guo, *Appl. Catal., B*, 2008, **79**, 307-312.
30. Q. Liu, J. Gao, M. Zhang, H. Li, F. Gu, G. Xu, Z. Zhong and F. Su, *RSC Adv.*, 2014, **4**, 16094-16103.

31. J. Gao, C. Jia, J. Li, F. Gu, G. Xu, Z. Zhong and F. Su, *Ind. Eng. Chem. Res.*, 2012, **51**, 10345-10353.
32. Q. Liu, J. Gao, F. Gu, X. Lu, Y. Liu, H. Li, Z. Zhong, B. Liu, G. Xu and F. Su, *J. Catal.*, 2015, **326**, 127-138.
33. C. Jia, J. Gao, J. Li, F. Gu, G. Xu, Z. Zhong and F. Su, *Catal. Sci. Technol.*, 2013, **3**, 490-499.
34. X. Lu, F. Gu, Q. Liu, J. Gao, Y. Liu, H. Li, L. Jia, G. Xu, Z. Zhong and F. Su, *Fuel Process. Technol.*, 2015, **135**, 34-46.
35. Y. Liu, J. Gao, Q. Liu, F. Gu, X. Lu, L. Jia, G. Xu, Z. Zhong and F. Su, *RSC Adv.*, 2015, **5**, 7539-7546.
36. K. Prabhakaran, J. James and C. Pavithran, *J. Eur. Ceram. Soc.*, 2003, **23**, 379-385.
37. X. Cai, X. Dong and W. Lin, *J. Nat. Gas Chem.*, 2008, **17**, 98-102.
38. Y.-S. Oh, H.-S. Roh, K.-W. Jun and Y.-S. Baek, *Int. J. Hydrogen Energy*, 2003, **28**, 1387-1392.
39. N. Wang, K. Shen, L. Huang, X. Yu, W. Qian and W. Chu, *ACS Catal.*, 2013, **3**, 1638-1651.
40. N. Wang, W. Chu, T. Zhang and X.-S. Zhao, *Chem. Eng. J.*, 2011, **170**, 457-463.
41. J. Liu, C. Li, F. Wang, S. He, H. Chen, Y. Zhao, M. Wei, D. G. Evans and X. Duan, *Catal. Sci. Technol.*, 2013, **3**, 2627-2633.
42. J. Gao, Y. Wang, Y. Ping, D. Hu, G. Xu, F. Gu and F. Su, *RSC Adv.*, 2012, **2**, 2358-2368.
43. J. Happel, I. Suzuki, P. Kokayeff and V. Fthenakis, *J. Catal.*, 1980, **65**, 59-77.
44. H. Li, Y. Xu, C. Gao and Y. Zhao, *Catal. Today*, 2010, **158**, 475-480.

### Figure Captions

**Fig. 1** Wide-angle XRD patterns of the support and fresh reduced catalysts: (a) SiC, (b) 20Ni80SiC, (c) 20Ni5Al75SiC, (d) 20Ni10Al70SiC, (e) 20Ni20Al60SiC (A), and the enlarged view of part of (A) marked with shadow (B).

**Fig. 2** SEM images of the samples: (a) SiC, (b) 20Ni80SiC, and (c) 20Ni10Al70SiC.

**Fig. 3** SEM image (a), the EDS element layered image (b) and elemental mapping images of Ni (c), Al (d), O (e) and Si (f) of 20Ni10Al70SiC.

**Fig. 4** TEM images of the reduced catalysts: (a) SiC, (b) 20Ni80SiC, (c and d) 20Ni10Al70SiC.

**Fig. 5** Ni 2p (a) and O 1s (b) XPS spectra of the fresh reduced 20Ni80SiC and 20Ni10Al70SiC.

**Fig. 6** H<sub>2</sub>-TPR profiles (a) of the support and reduced catalysts and H<sub>2</sub>-TPD profiles (b) of the reduced catalysts.

**Fig. 7** Catalytic performances of catalysts in CO methanation under different reaction temperatures at 0.1 MPa and WHSV of 30 000 mL g<sup>-1</sup> h<sup>-1</sup>: (a) CO conversion, (b) CH<sub>4</sub> selectivity, and (c) CH<sub>4</sub> yield.

**Fig. 8** Arrhenius plots for CO methanation over all the catalysts.

**Fig. 9** Lifetime test of 20Ni80SiC, 20Ni5Al75SiC and 20Ni10Al70SiC for CO methanation: (a) CO conversion, (b) CH<sub>4</sub> selectivity and (c) CH<sub>4</sub> yield.

**Fig. 10** TEM images of the used catalysts after lifetime test: (a) 20Ni80SiC, (b) 20Ni5Al75SiC, (c) 20Ni10Al70SiC, and (d) TG curves of the used 20Ni80SiC and 20Ni10Al70SiC.

**Fig. 11** Catalytic activities of 20Ni80SiC and 20Ni10Al70SiC for CO methanation after hydrothermal treatment: (a) CO conversion, (b) CH<sub>4</sub> selectivity and (c) CH<sub>4</sub> yield.

**Table 1** Physical and chemical properties of the catalysts

Samples	$S_{\text{BET}}^a$	$V_p^b$	$D_p^c$	Ni Particle size (nm)		H <sub>2</sub> uptake	$D^e$	$TOF^f$
	(m <sup>2</sup> g <sup>-1</sup> )	(cm <sup>3</sup> g <sup>-1</sup> )	(nm)	By XRD <sup>d</sup>	By TEM	(μmol g <sup>-1</sup> )	(%)	(260°C)/s <sup>-1</sup>
20Ni80SiC	23	0.045	15.1	13.3	15.2	57.5	4.3	0.062
20Ni5Al75SiC	44	0.067	4.3	7.3	11.3	139.0	9.8	0.110
20Ni10Al70SiC	52	0.062	3.8	5.5	8.4	141.4	10.6	0.158
20Ni20Al60SiC	84	0.090	4.6	5.9	9.0	136.0	10.2	0.123

<sup>a</sup> Surface area derived from BET equation.

<sup>b</sup> Pore volume obtained from the volume of nitrogen adsorbed at the relative pressure of 0.97.

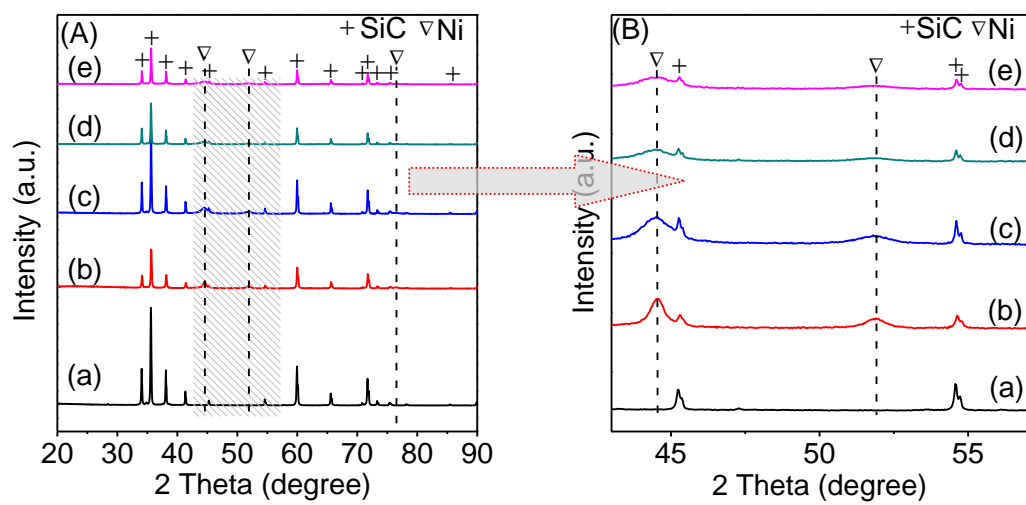
<sup>c</sup> pore size derived from BJH method using adsorption branch.

<sup>d</sup> Estimated from the XRD diffraction peak ( $2\theta = 44.6$ ) using the Debye-Scherrer equation.

<sup>e</sup> Ni dispersion calculated based on the H<sub>2</sub>-TPR and H<sub>2</sub>-TPD results.

<sup>f</sup> Calculated based on the metal dispersion and the CO conversion at 260 °C.

Fig. 1



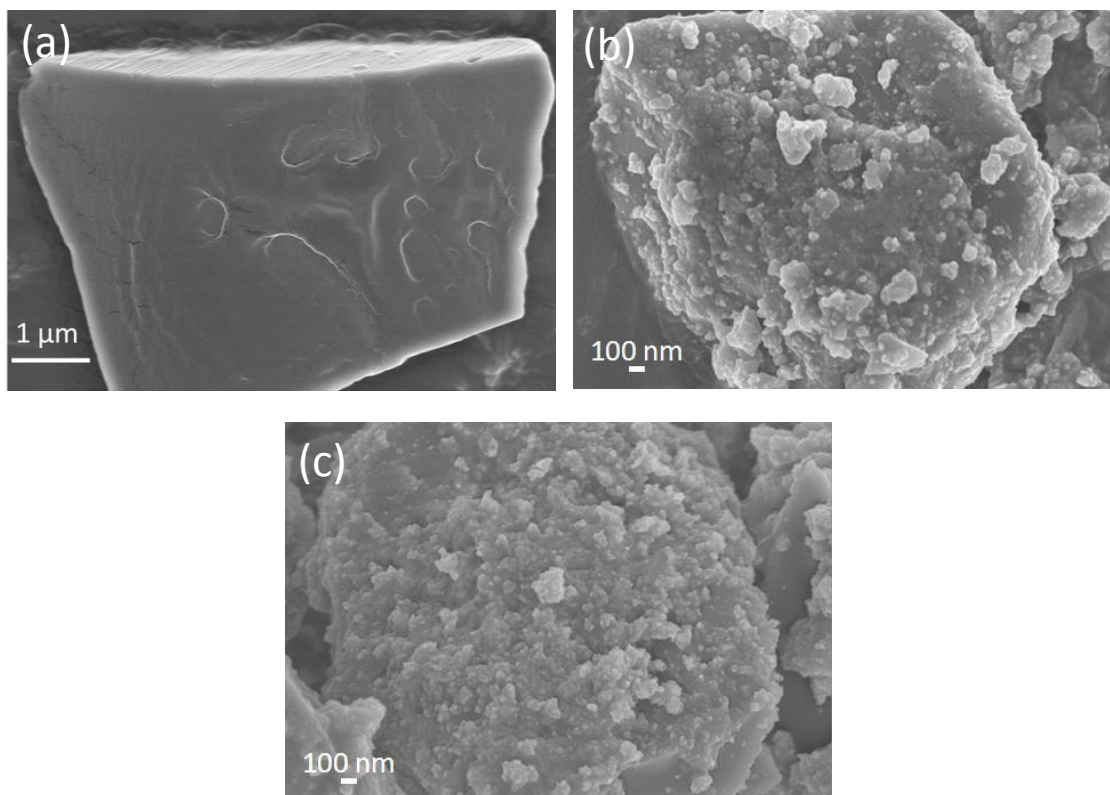
**Fig. 2**

Fig. 3

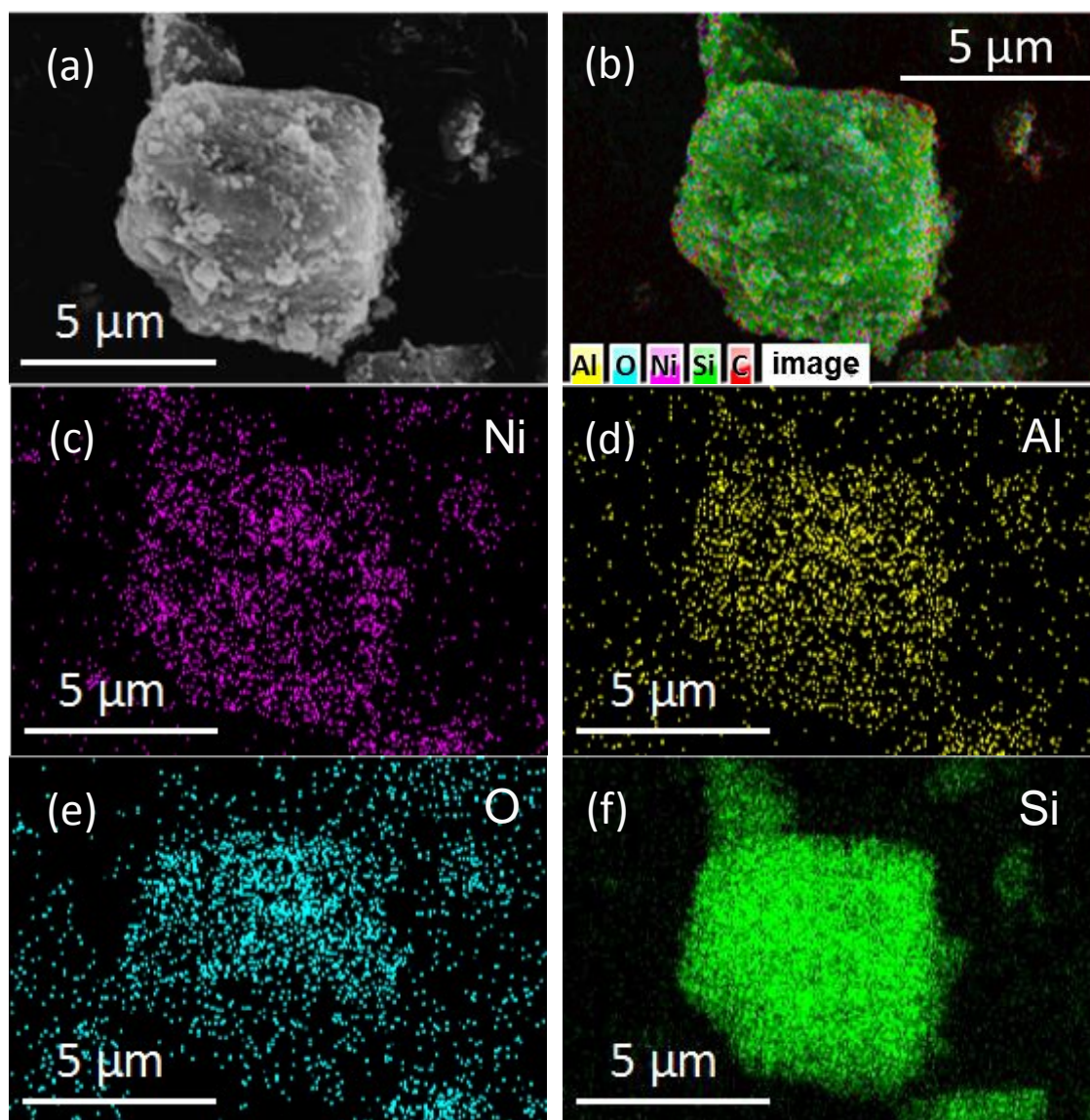


Fig. 4

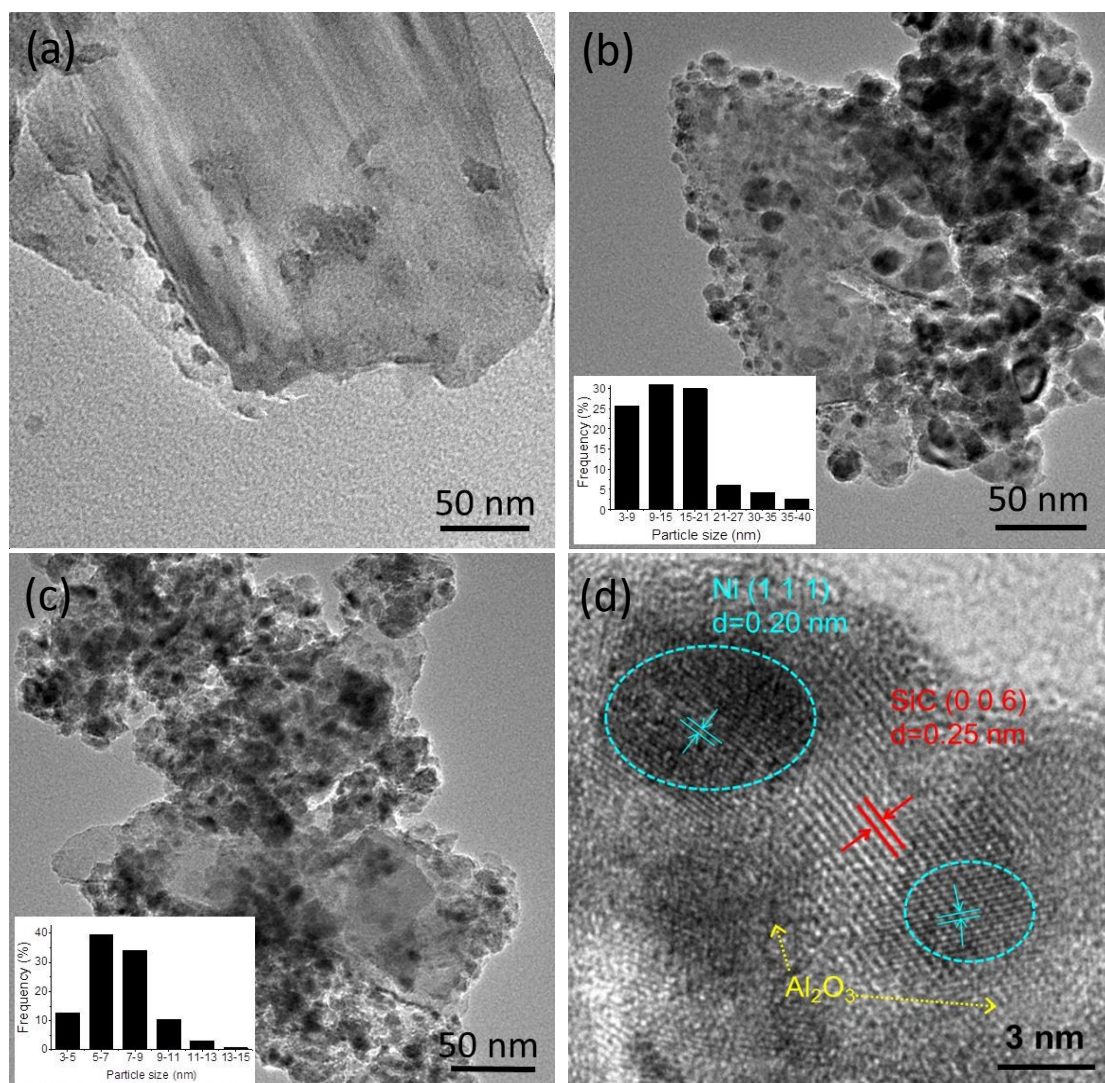


Fig.5

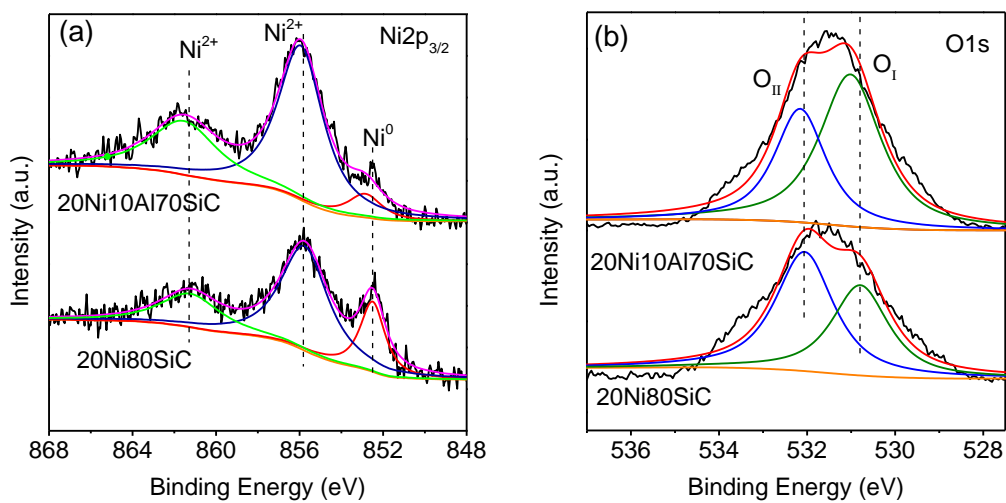


Fig. 6

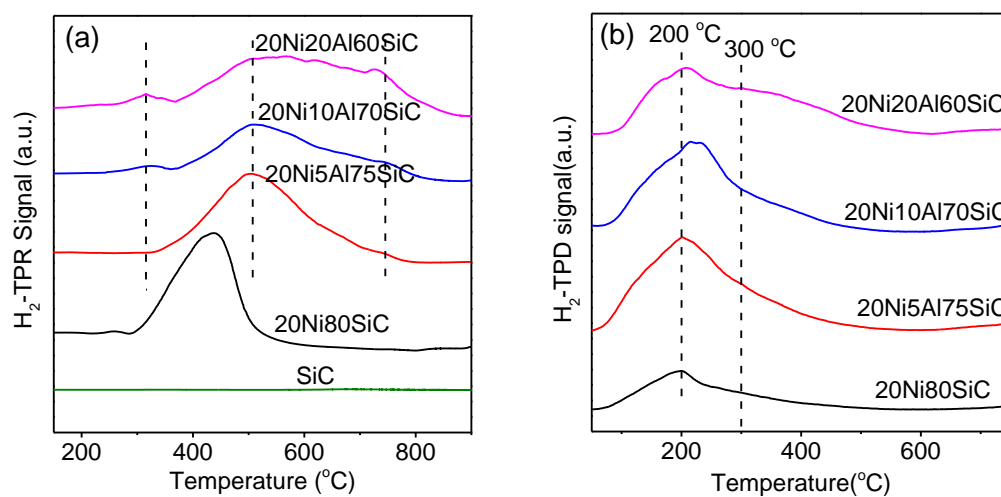


Fig. 7

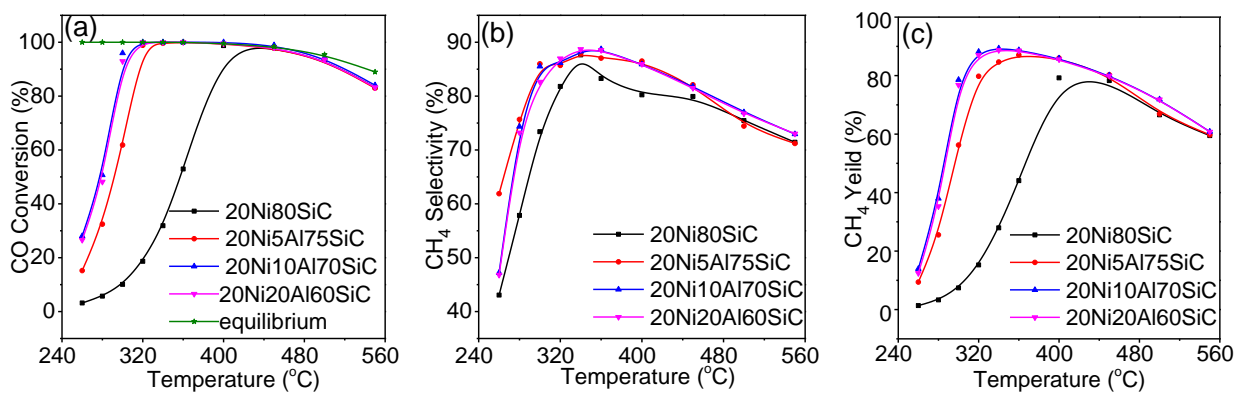


Fig. 8

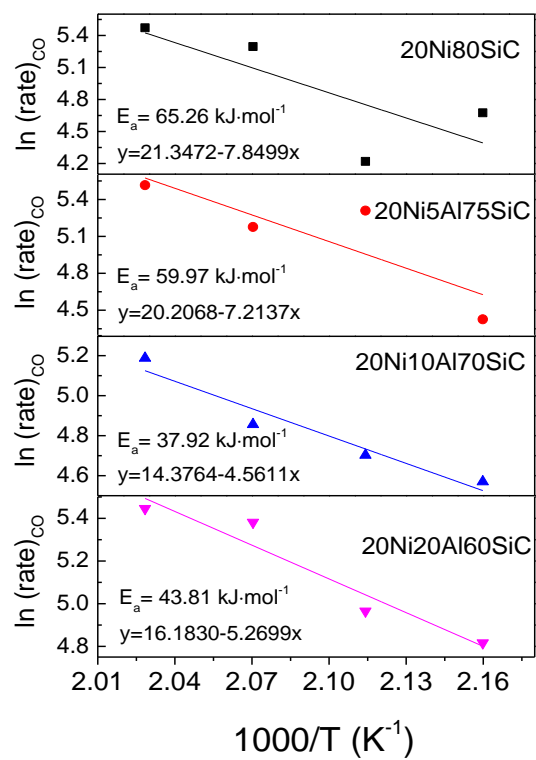


Fig. 9

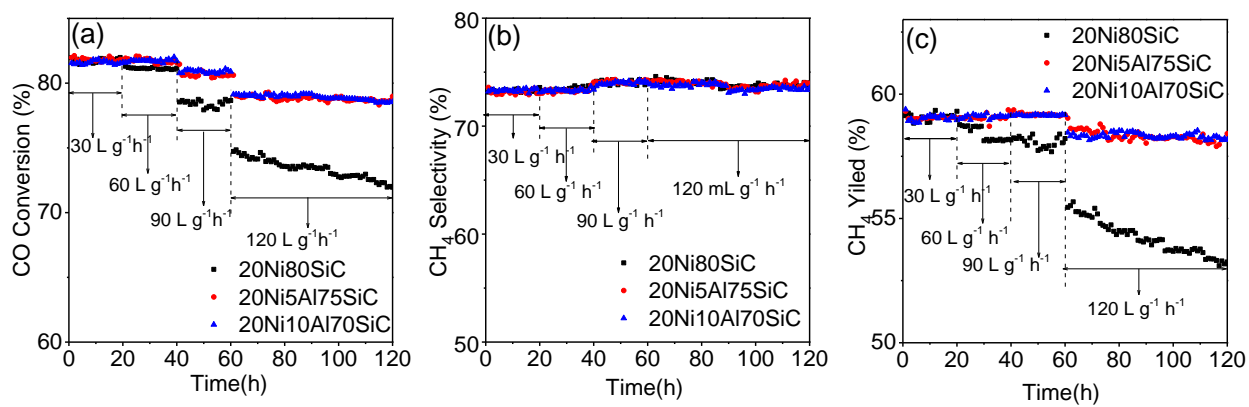


Fig. 10

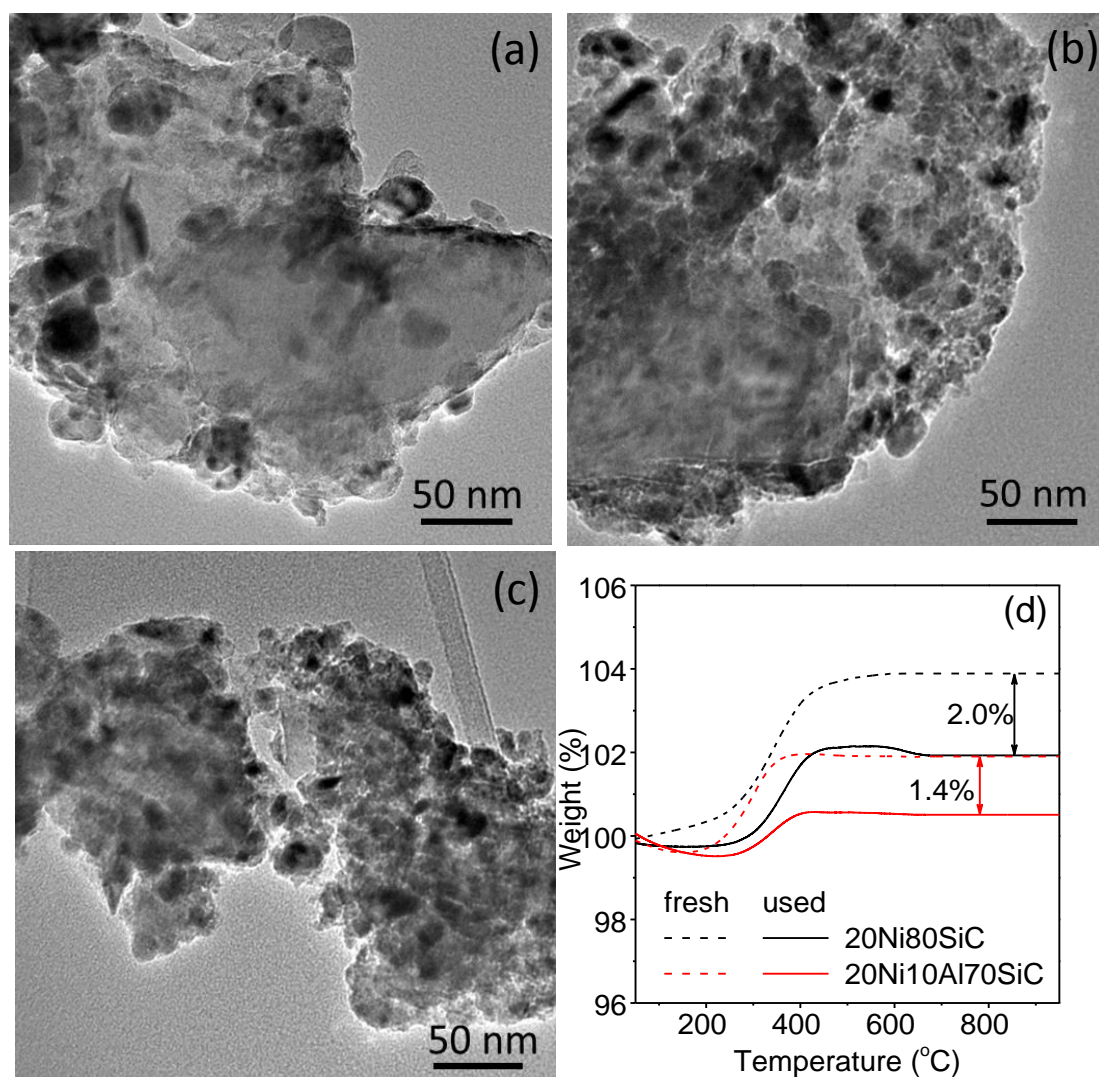
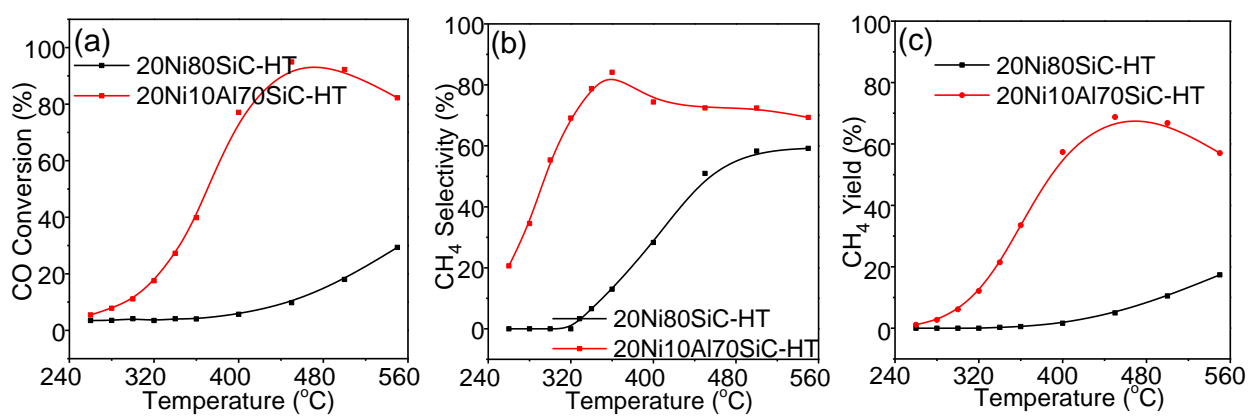


Fig. 11



## Graphical Abstract

Ni/SiC-A<sub>2</sub>O<sub>3</sub> exhibits good catalytic activity and stability due to excellent heat conductivity of SiC and enhanced interactions between Ni and support by alumina modification, thus inhibiting the migration of Ni particles.

